Depletion of the Receptor-Interacting Protein Kinase 3 (RIP3) Decreases Photoreceptor Cell Death During the Early Stages of Ocular Murine Cytomegalovirus Infection

Jinxian Xu,[1,2] Juan Mo,[1] Xinglou Liu,[1,2] Brendan Marshall,[1] Sally S. Atherton,[1] Zheng Dong,[1] Sylvia Smith,[1,2] and Ming Zhang[1,2]

[1]Department of Cellular Biology and Anatomy, Medical College of Georgia, Augusta University, Augusta, Georgia, United States
[2]James and Jean Vision Discovery Institute, Medical College of Georgia, Augusta University, Augusta, Georgia, United States

Correspondence: Ming Zhang, Department of Cellular Biology and Anatomy, Augusta University, R and E Building, Room CB2815, Augusta, GA 30912, USA; mzhang@augusta.edu.

JX and JM contributed equally to the work presented here and should therefore be regarded as equivalent authors.

Submitted: February 12, 2017
Accepted: April 13, 2018

Citation: Xu J, Mo J, Liu X, et al. Depletion of the receptor-interacting protein kinase 3 (RIP3) decreases photoreceptor cell death during the early stages of ocular murine cytomegalovirus infection. *Invest Ophthalmol Vis Sci*. 2018;59:2445–2458. https://doi.org/10.1167/iovs.18-24086

Purpose. The purpose of this study was to determine if the receptor-interacting protein kinase 3 (RIP3) plays a significant role in innate immune responses and death of bystander retinal neurons during murine cytomegalovirus (MCMV) retinal infection, by comparing the innate immune response and cell death in RIP3-depleted mice ($Rip3^{-/-}$) and $Rip3^{+/+}$ control mice.

Methods. $Rip3^{-/-}$ and $Rip3^{+/+}$ mice were immunosuppressed (IS) and inoculated with MCMV via the supraciliary route. Virus-injected and mock-injected control eyes were removed at days 4, 7, and 10 post infection (p.i.) and markers of innate immunity and cell death were analyzed.

Results. Compared to $Rip3^{+/+}$ mice, significantly more MCMV was recovered and more MCMV-infected RPE cells were observed in injected eyes of $Rip3^{-/-}$ mice at days 4 and 7 p.i. In contrast, fewer TUNEL-stained photoreceptors were observed in $Rip3^{-/-}$ eyes than in $Rip3^{+/+}$ eyes at these times. Electron microscopy showed that significantly more apoptotic photoreceptor cells were present in $Rip3^{+/+}$ mice than in $Rip3^{-/-}$ mice. Immunohistochemistry showed that the majority of TUNEL-stained photoreceptors died via mitochondrial flavoprotein apoptosis-inducing factor (AIF)-mediated, caspase 3–independent apoptosis. The majority of RIP3-expressing cells in infected eyes were RPE cells, microglia/macrophages, and glia, whereas retinal neurons contained much lower amounts of RIP3. Western blots showed significantly higher levels of activated nuclear factor–κB and caspase 1 were present in $Rip3^{+/+}$ eyes compared to $Rip3^{-/-}$ eyes.

Conclusions. Our results suggest that RIP3 enhances innate immune responses against ocular MCMV infection via activation of the inflammasome and nuclear factor–κB, which also leads to inflammation and death of bystander cells by multiple pathways including apoptosis and necroptosis.

Keywords: apoptosis, murine cytomegalovirus, innate immune response, retinitis

Human cytomegalovirus (HCMV) is a ubiquitous virus, which is normally kept in check by a healthy immune system. However, compromise of the immune system, either deliberately, such as in immunosuppressed organ transplant patients, or naturally, such as in individuals infected with human immunodeficiency virus (HIV), may result in HCMV morbidity due to virus activation, leading to various clinical sequelae, including retinitis. HCMV retinitis is a serious ocular complication of HIV infection, and prior to development of combination antiretroviral therapy (cART),[1–5] occurred in ~30% of HIV/AIDS patients. Although its incidence has diminished as a result of cART, it nevertheless remains a significant problem. In recent years, numerous reports have also linked HCMV retinitis with HIV-negative patients[6] while the occurrence of HCMV retinitis in immunosuppressed (IS) patients who were undergoing solid-organ or bone marrow transplantation has also been accumulating.[7,8] Microscopic analysis of human ocular tissue obtained postmortem, combined with close clinical analysis of patients, has provided some information on the pathogenesis of HCMV in the retina. However, since the human retina is not amenable to experimental manipulation, animal models have been invaluable in dissecting the progression of viral destruction of retinal tissue. The murine counterpart of HCMV, murine cytomegalovirus (MCMV), has been widely studied in this regard, both by ourselves and others, and the murine model has provided considerable data that have led to a deeper understanding of virus-induced cell death.[9,10]

The model utilized in our laboratory involves intraocular injection of MCMV via the supraciliary route following steroid-induced immunosuppression. This results in a retinal infection with similar pathogenic characteristics to those noted in human ocular specimens infected with HCMV.[11–13] Our model has demonstrated that early in infection, MCMV is localized to discrete types of retinal neurons such as horizontal cells and bipolar cells,[13] whereas amacrine cells, photoreceptors, and ganglion cells show little evidence of MCMV infection.[13] MCMV completes its replication cycle with the help of several virus-encoded proteins, which ensure survival of the host cell by inhibiting programmed cell death pathways such as apoptosis

and necroptosis. As a result, viral progeny are produced and infection spreads to surrounding cells.[14–16] In contrast, nearby uninfected cells undergo cell death leading to drastic disruption of retinal structure, and substantial evidence now supports the hypothesis that death of uninfected bystander neuronal cells plays an important role in the pathogenesis of CMV retinitis.[12,13,17–24] The receptor-interacting protein (RIP) homotypic interaction motif (RHIM)-containing signaling adaptors, RIP1 and RIP3, are key decision makers in cell death and innate immunity,[5,18] and since production of RIP3 is greatly increased post ocular MCMV infection,[25,26] we hypothesized that RIP3 might play an important role in both the innate immune response and the death of uninfected retinal cells. Therefore, the purpose of this study was to test this hypothesis by comparing the pathogenesis of MCMV retinal infection in *Rip3*$^{-/-}$ and wild-type control mice.

Materials and Methods

Virus and Virus Titration

MCMV strain K181 was kindly supplied by Edward Morcarski, Emory University, Atlanta, Georgia, USA. Virus preparation from salivary glands of MCMV-infected BALB/c mice has been previously described[11] together with methods of viral titer determination by plaque assay and virus storage.

Mice

Breeding pairs of *Rip3*$^{-/-}$ mice and control C57BL/6 (*Rip3*$^{+/+}$) mice were purchased from Genentech Corp. (San Francisco, CA, USA). All the mice tested negative by PCR for the rd8 mutation. National Institutes of Health guidelines for the care and maintenance of mice and the ARVO Statement for the Use of Animals in Ophthalmic and Vision Research were followed in all experiments. All experimental protocols were approved by the Institutional Animal Care and Use Committee of Augusta University. Typically, 6- to 8-week-old adult mice were used in all experiments. Anesthesia protocols have been described previously.[25]

Antibodies

Anti-MCMV early antigen (EA)[27] was used to identify MCMV-infected cells. The preparation and use of FITC-labeled anti-MCMV EA has been described elsewhere.[13] Rat anti-glycine antibody (specific for amacrine cells) was kindly provided by David V. Pow, University of Queensland, Australia. Mouse anti-IBA1 (specific for macrophages/microglia) was from Wako, Inc. (Richmond, VA, USA). Mouse anti-rhodopsin (specific for photoreceptors) was from Abcam (Cambridge, MA, USA). Mouse anti-GFAP (glial fibrillary acidic protein, specific for glia/Müller cells), FITC-labeled anti-CD11b (specific for macrophages/microglia), FITC-labeled anti-CD3 (specific for CD3^{+} T cells), and FITC-labeled anti-Gr-1 (specific for neutrophils) were all from BD Biosciences (San Jose, CA, USA). Anti-cleaved caspase 3, anti-AIF (apoptosis-inducing factor), anti-caspase 1, anti-poly(ADP-ribose)polymerase 1 (PARP1), anti-nuclear factor–κB (NF-κB), anti-RIP3, goat anti-rabbit IgG-horseradish peroxidase (HRP), and goat anti-mouse IgG-HRP were all from Cell Signaling (Cell Signaling Technology, Inc., Danvers, MA, USA). Anti-β-actin was from Sigma-Aldrich Corp. (St. Louis, MO, USA). Biotin-labeled anti-rat IgG (mouse serum absorbed), anti-mouse Alexa 488, anti-rabbit Alexa 594, AMCA-labeled avidin, FITC-labeled avidin, and Texas red–labeled avidin were from Vector Laboratories, Inc. (Burlingame, CA, USA).

Experimental Plan

Mice were IS by intramuscular injection of 2.0 mg sterile methylprednisolone acetate suspension every 3 days beginning on day –2 according to our usual protocol.[13,23,25] This protocol typically depletes 93% of T cells (CD4^{+}, CD8^{+}) and macrophages from MCMV-infected mice as measured by flow cytometry of splenocytes. Ocular virus infection of mice was carried out with 1×10^4 plaque-forming unit (PFU) MCMV as previously described.[23,25] Eyes, salivary gland, lung, and liver were removed and prepared for measurement of virus titer by plaque assay while electron microscopy, immunohistochemistry, and Western blots were performed on eyes of additional mice.

Immunofluorescence Staining

Injected eyes were fixed in 4% paraformaldehyde (Electron Microscopy Sciences, Hatfield, PA, USA) for 30 minutes, immersed in 25% sucrose overnight, snap frozen, and sectioned on a cryostat. At least four slides (each slide representing one injected eye) in each group were used for each type of staining. In single- and double-staining experiments, slides were mounted with antifade medium containing 4′,6-diamidino-2-phenylindole (DAPI; Vectashield, Vector Laboratories) to visualize nuclei and images were captured using a confocal microscope (Zeiss upright 780; Oberkochen, Germany).

For double staining with TUNEL and MCMV EA, sections were initially stained with TUNEL (in Situ Cell Death Detection Kit, Fluorescein; Roche Diagnostics, Indianapolis, IN, USA) according to the manufacturer's instructions. After washing and blocking, biotinylated anti-EA (1:500) was applied to the section overnight, followed by Texas red–labeled avidin (1:600) for 1 hour at room temperature.

For double staining with TUNEL and AIF, sections were initially stained with TUNEL as described above. After washing and blocking, sections were incubated overnight at 4°C in rabbit-derived anti-AIF, followed by Alexa 594–labeled anti-rabbit IgG (1:1000) for 1 hour at room temperature.

For double staining of RIP3 and retinal antigens, slides were washed for 30 minutes in PBS followed by permeabilization with 0.1% Triton X-100 in 0.1% sodium citrate for 2 minutes on ice. After blocking in PBS containing 10% normal goat serum, 2% BSA, and 0.5% Triton X-100 for 1 hour, sections were incubated overnight at 4°C in primary antibody, rabbit-derived anti-RIP3 (1:200). Following washing, sections were incubated with anti-rabbit Alexa 594 (1:1000) for 1 hour at room temperature, washed, and then stained for different retinal antigens; GFAP was used to identify glia, rhodopsin was used to stain photoreceptors, and IBA1 was used to identify microglia. For antibodies raised in mice including anti-GFAP (1:200), anti-rhodopsin (1:100), and anti-IBA1 (1:100), each mouse-derived primary antibody was mixed with biotinylated anti-mouse secondary antibody (ARK; Dako Corp., Carpinteria, CA, USA). After 15 minutes, the blocking reagent (ARK), containing normal mouse serum, was added to the mixture. Mouse immunoglobulin in the blocking reagent bound to the biotinylated anti-mouse antibody that was not bound to primary antibody, thus minimizing reactivity with endogenous immunoglobulin in the specimen. The biotin-labeled primary antibody was then applied to the section. Staining was completed by addition of FITC-avidin (1:600) for 1 hour at room temperature.

For double staining of RIP3 and cellular antigens (CD3, CD11b, and Gr-1) or viral EA for which the antibodies were directly labeled with FITC, sections were initially stained with RIP3 as described above, then incubated with the relevant

Investigative Ophthalmology & Visual Science

FITC-labeled antibody (1:50) overnight at 4°C. For double staining with TUNEL and RIP3, sections were first stained by TUNEL assay, washed, and then stained with RIP3 as described above.

For triple staining with TUNEL, RIP3, and rhodopsin, sections were first stained with TUNEL and RIP3 as described above, then incubated with mouse anti-rhodopsin (1:100) overnight at 4°C, also as described above. Staining was completed by addition of AMCA-avidin (1:200) at room temperature for 1 hour.

For quantitation of RIP3 staining in each type of ocular cell, 40 fields were chosen randomly from four slides (each slide representing one eye) under a fluorescence microscope for each double staining, and two images were acquired from red and green fluorescence channels, respectively, in each field. The number of RIP3-stained red cells and green-stained specific retinal cells, as well as double-stained cells (yellow in merged images), was quantitated in all fields. The total number of each of these three types of stained cells was used to calculate the percentage of RIP3-stained retinal cell types.

Western Blot Analysis

Western blotting was performed as previously described.[12,19,23,25] Briefly, proteins were extracted from MCMV-injected or mock-injected eyes and equal amounts of proteins were separated by SDS-PAGE, followed by electroblotting onto polyvinylidene difluoride (PVDF) membranes (GE Healthcare, Piscataway, NJ, USA). Following blocking with 5% nonfat dry milk for 1 hour at room temperature, membranes were incubated overnight at 4°C with primary antibodies (as shown in the "Antibody" section in Methods, at the dilution of 1:1000 with 5% BSA) and for 1 hour at room temperature with HRP-conjugated secondary antibody. Immune complexes were detected using chemiluminescence (ECL; GE Healthcare) and exposure to x-ray film. To verify equal loading among lanes, membranes were probed with anti-β-actin. ImageJ (National Institutes of Health, Bethesda, MD, USA) was used to quantify signal intensity.

Electron Microscopy (EM)

Fixation of eyes from experimental and control mice (three eyes per group) was performed by immersion in a solution of 2% glutaraldehyde, 2% paraformaldehyde, and 0.1 M cacodylate at 4°C overnight. Eyes were then washed in 0.1 M cacodylate and postfixed with 4% osmium tetroxide for 1 hour at room temperature prior to dehydration in a graded ethanol series. Eyes were embedded in Pure Embed 812 mixture (Electron Microscopy Sciences), and 70-nm sections were stained with uranyl acetate and lead citrate prior to visualization in a JEM 1230 electron microscope (JEOL, Tokyo, Japan). Quantification of apoptotic cells was performed by counting the number of apoptotic cells in a 45 × 45-μm area of the electron micrographs, and values were expressed as mean ± SEM.

Retinitis Scoring

To analyze the extent of retinopathy at late-stage infection, additional frozen sections of injected eyes at day 10 post infection (p.i.) were fixed with 4% paraformaldehyde for 15 minutes and stained with hematoxylin and eosin (H&E). Changes in the posterior segment of each section were evaluated microscopically as previously described.[11,28] The highest posterior segment score for each eye was the retinal score and was used to determine the mean retinal score. Data were analyzed as described below.

Statistical Analysis

All data were expressed as means ± SEM (standard error of mean), where n is the number of mice or number of fields used in each experimental group. Statistical significance was determined using either a 2-tailed t-test or ANOVA using the GraphPad Prism 6 analysis tool (GraphPad Software, Inc., San Diego, CA, USA). P values < 0.05 were deemed significant.

Results

Depletion of RIP3 Increases Viral Spread and Replication but Reduces Death of Photoreceptor Cells at Early Stages of Infection

Following immunosuppression and virus inoculation, MCMV-positive cells were found in the anterior segment and RPE layer of both $Rip3^{-/-}$ and $Rip3^{+/+}$ mice at day 4 p.i. (Fig. 1, A1, A2). At this time, TUNEL-positive staining was observed in uninfected photoreceptor cells, especially in areas of the retina where the subjacent RPE cells were MCMV infected, as we have previously described.[18,19,23] Compared to wild-type mice, significantly more MCMV was recovered (Fig. 1B) and more MCMV-infected RPE cells were present in injected eyes of $Rip3^{-/-}$ mice (Fig. 1, A1, A2). In contrast, fewer TUNEL-positive photoreceptors were observed in MCMV-injected eyes of $Rip3^{-/-}$ mice compared to injected eyes of $Rip3^{+/+}$ mice (Fig. 1, A1, A2). Previous data from our laboratory have shown that death of photoreceptor cells is temporally associated with the spread of MCMV from the initial site of infection in the RPE layer to Müller cells during progression of MCMV retinitis.[13] Probably because of less photoreceptor cell death, widespread RPE infection in $Rip3^{-/-}$ eyes did not result in an earlier spread of MCMV from the RPE to inner retina, since at day 7 p.i. (Fig. 1, A3, A4), similar numbers of virus-infected cells were observed in the inner retinas of $Rip3^{-/-}$ and $Rip3^{+/+}$ mice. TUNEL-positive cells were also observed in the inner retina, with the majority being uninfected bystander retinal cells. Fewer TUNEL-positive cells were observed in the inner retina of $Rip3^{-/-}$ (Fig. 1, A4) compared to $Rip3^{+/+}$ eyes (Fig. 1, A3). However, by day 10 p.i., significantly more MCMV was recovered (Fig. 1B) and more infected retinal cells were noted in $Rip3^{-/-}$ injected eyes (Fig. 1, A6), compared to $Rip3^{+/+}$ injected eyes (Fig. 1, A5). Not surprisingly, many TUNEL-positive cells were observed in the inner retina of both $Rip3^{-/-}$ and $Rip3^{+/+}$ eyes at that time point (Fig. 1, A5, A6). We also measured viral titers in extraocular tissues at day 10 post intraocular MCMV infection. In contrast to MCMV replication in the eyes (Fig. 1B), we observed no significant differences of viral titers in salivary glands, livers, or lungs between $Rip3^{-/-}$ and control $Rip3^{+/+}$ mice (Fig. 1C).

Since more MCMV was recovered and more infected retinal cells were present in $Rip3^{-/-}$ infected eyes compared to $Rip3^{+/+}$ infected eyes at day 10 p.i., the extent of retinopathy might eventually be exacerbated in $Rip3^{-/-}$ mice. To test this hypothesis, sections of MCMV-infected eyes were prepared at day 10 p.i. and stained with H&E. Compared to $Rip3^{+/+}$ infected eyes (Fig. 2, A1), more cytomegalic cells and increased disruption of retinal architecture were observed in $Rip3^{-/-}$ infected eyes (Fig. 2, A2). The average retinitis score of eyes of IS $Rip3^{-/-}$ mice was higher than that of IS $Rip3^{+/+}$ mice (Fig. 2, A3).

Electron Microscopy

To determine if depletion of RIP3 reduces photoreceptor death by apoptosis or necrosis at early stages of MCMV ocular

Investigative Ophthalmology & Visual Science

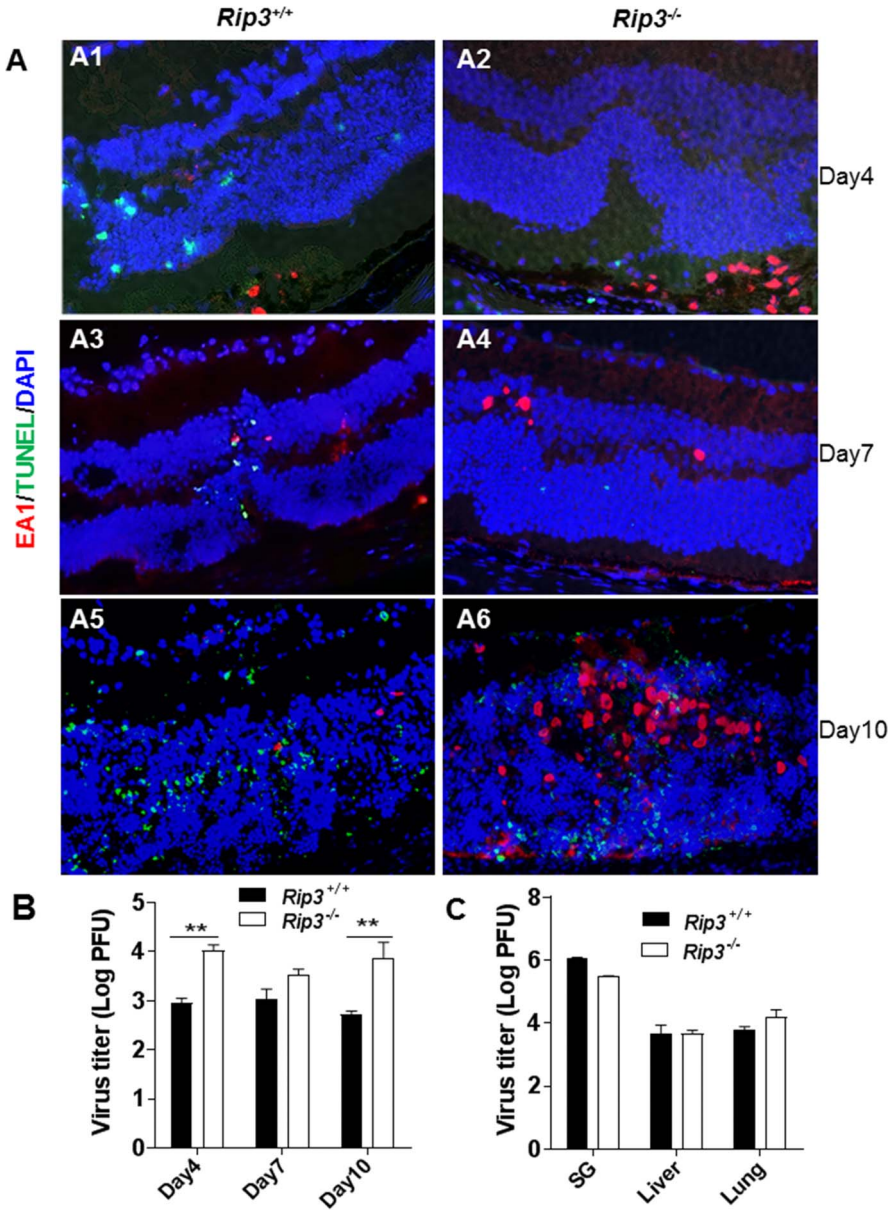

Figure 1. (**A**) Merged photomicrographs of staining for MCMV EA (*red*), TUNEL (*green*), and DAPI (*blue*) in MCMV-injected eyes of IS $Rip3^{-/-}$ and $Rip3^{+/+}$ mice at days 4, 7, and 10 p.i. Fewer TUNEL-stained cells were observed in the inner retina of $Rip3^{-/-}$ (**A2**, **A4**) compared to $Rip3^{+/+}$ eyes (**A1**, **A3**) at days 4 and 7 p.i. At day 10 p.i., more infected retinal cells were observed in the injected eyes of $Rip3^{-/-}$ mice (**A6**) than in the injected eyes of $Rip3^{+/+}$ mice (**A5**), and many TUNEL-positive cells were observed in the inner retina of both $Rip3^{-/-}$ and $Rip3^{+/+}$ eyes. (**B**) Titer of MCMV (log10 ± SEM PFU/mL) in MCMV-injected eyes of $Rip3^{-/-}$ and $Rip3^{+/+}$ mice at days 4, 7, and 10 p.i. Data are shown as mean ± SEM ($n = 4$). Statistical analysis by 2-tailed *t*-test. $^{**}P < 0.01$. (**C**) Titer of MCMV (log10 ± SEM PFU/mL) in salivary glands, livers, and lungs of IS $Rip3^{-/-}$ and $Rip3^{+/+}$ mice at day 10 p.i. Statistical analysis by 2-tailed *t*-test indicated no significant difference between $Rip3^{-/-}$ and $Rip3^{+/+}$ mice.

infection, additional injected eyes were collected at day 7 p.i. and prepared for EM. Considerable numbers of apoptotic photoreceptor cells were present in the outer nuclear layer of MCMV-infected $Rip3^{+/+}$ wild-type mice (Fig. 2, B1, indicated by arrow). These photoreceptor cells exhibited typical apoptotic features including condensation of chromatin and reduction of nuclear volume.[13] Additionally, cells at a more advanced stage of apoptosis were also noted and typically exhibited more extensive chromatin condensation and increased cell shrinkage. A few necrotic photoreceptor cells that exhibited marked lytic changes in cytoplasm and organelles were also noted (Fig. 2, B1, indicated by arrowheads). In addition, a relatively small number of photoreceptor cells in MCMV-infected $Rip3^{+/+}$ eyes exhibited nuclear shrinkage and strong chromatin condensation as well as cytoplasmic lysis (Fig. 2, B3, indicated by arrows) typical of AIF-mediated necroptotic death (also called parthanatos[29]). Compared to MCMV-infected $Rip3^{+/+}$ eyes, significantly fewer apoptotic photoreceptor cells were observed in the outer nuclear layer of $Rip3^{-/-}$ mice (Fig. 2, B2, B4). In addition, necrotic and necroptotic cells were rarely observed in the outer nuclear layer of $Rip3^{-/-}$ mice (Fig. 2, B2).

AIF-Mediated Caspase-Independent Cell Death

To determine if these apoptotic photoreceptor cells were caspase dependent or caspase independent, sections of MCMV-infected and mock-injected eyes were stained with anti-cleaved caspase 3 antibody and subjected to TUNEL assay. The results

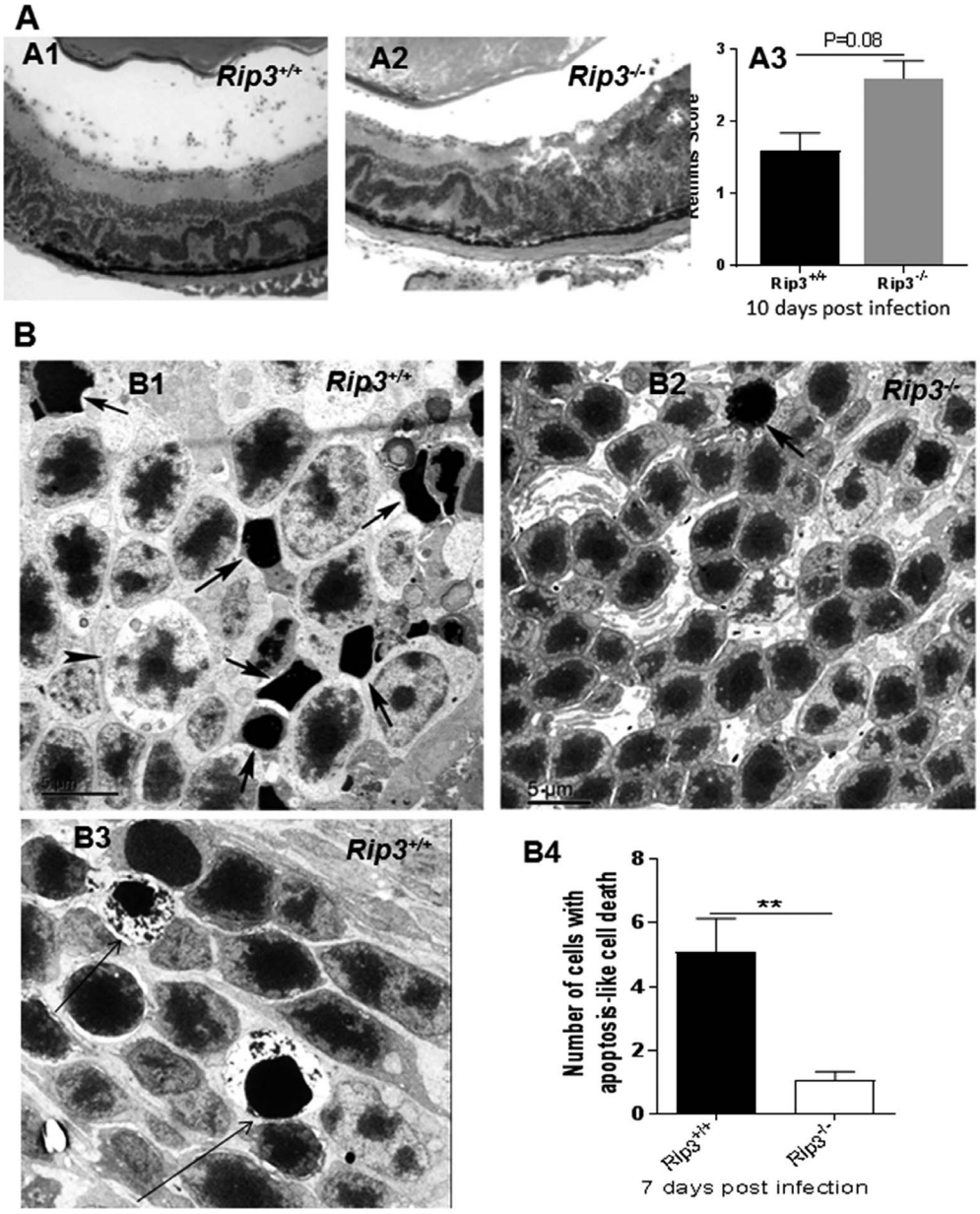

Figure 2. (**A**) Photomicrographs of hematoxylin- and eosin-stained sections of MCMV-infected eyes of an IS *Rip3*$^{+/+}$ mouse (**A1**) and an IS *Rip3*$^{-/-}$ mouse (**A2**) at day 10 p.i. Compared to *Rip3*$^{+/+}$ infected eyes (**A1**), more cytomegalic cells and increased disruption of retinal architecture were observed in *Rip3*$^{-/-}$ infected eyes (**A2**). Scoring of retinitis in MCMV-infected eyes of IS *Rip3*$^{+/+}$ and *Rip3*$^{-/-}$ mice at day 10 p.i. (**A3**). Data are shown as mean ± SEM ($n = 5$) and compared by a 2-tailed *t*-test ($P = 0.08$). (**B**) Electron micrographs of photoreceptors showing features typical of apoptosis (nuclear shrinkage and strong chromatin condensation, *arrows*) in the outer nuclear layer of the MCMV-injected eye of an IS *Rip3*$^{+/+}$ (**B1**) and an IS *Rip3*$^{-/-}$ mouse (**B2**) at day 7 p.i. A few necrotic photoreceptor cells that feature marked lytic changes in cytoplasm and organelles were also noted in *Rip3*$^{+/+}$ eyes (**B1**, indicated by *arrowhead*). A few AIF-mediated necroptotic photoreceptors, exhibiting nuclear shrinkage and strong chromatin condensation as well as cytoplasmic lysis, were also noted in *Rip3*$^{+/+}$ eyes (**B3**, *arrows*). (**B4**) Quantification of photoreceptor cells with apoptotic features in retinas of MCMV-injected *Rip3*$^{+/+}$ and *Rip3*$^{-/-}$ eyes at day 7 p.i. Data are shown as mean ± SEM ($n = 12$ fields) and compared by a 2-tailed *t*-test. $^{**}P < 0.01$.

showed that no cleaved caspase 3– or TUNEL-stained cells were present in the retina of control uninfected eyes (Fig. 3A) while only a small number of cleaved caspase 3–stained cells were observed in the inner retinas of MCMV-injected eyes (Fig. 3B), suggesting that the majority of TUNEL-stained photoreceptors died through a caspase-independent mechanism.

AIF mediates a caspase-independent programmed cell death pathway in which AIF is released from the mitochondrial intermembrane space following calpain activation[29–32] or overactivation of PARP1,[33–36] before being translocated to the nucleus where it induces apoptosis-like cell death.[29,30] Since depletion of RIP3 greatly decreased caspase-independent apoptosis-like cell death in photoreceptors (Fig. 2, B4), we hypothesized that AIF might induce photoreceptor cell death during MCMV retinitis. To determine if AIF was translocated to the nucleus of photoreceptors during MCMV retinitis, sections of MCMV-injected eyes and mock-injected control eyes were stained by TUNEL assay and for AIF. As shown in Figure 3C, AIF was not colocalized with nuclear DAPI staining in mock-injected control eyes, whereas in MCMV-infected eyes, AIF was

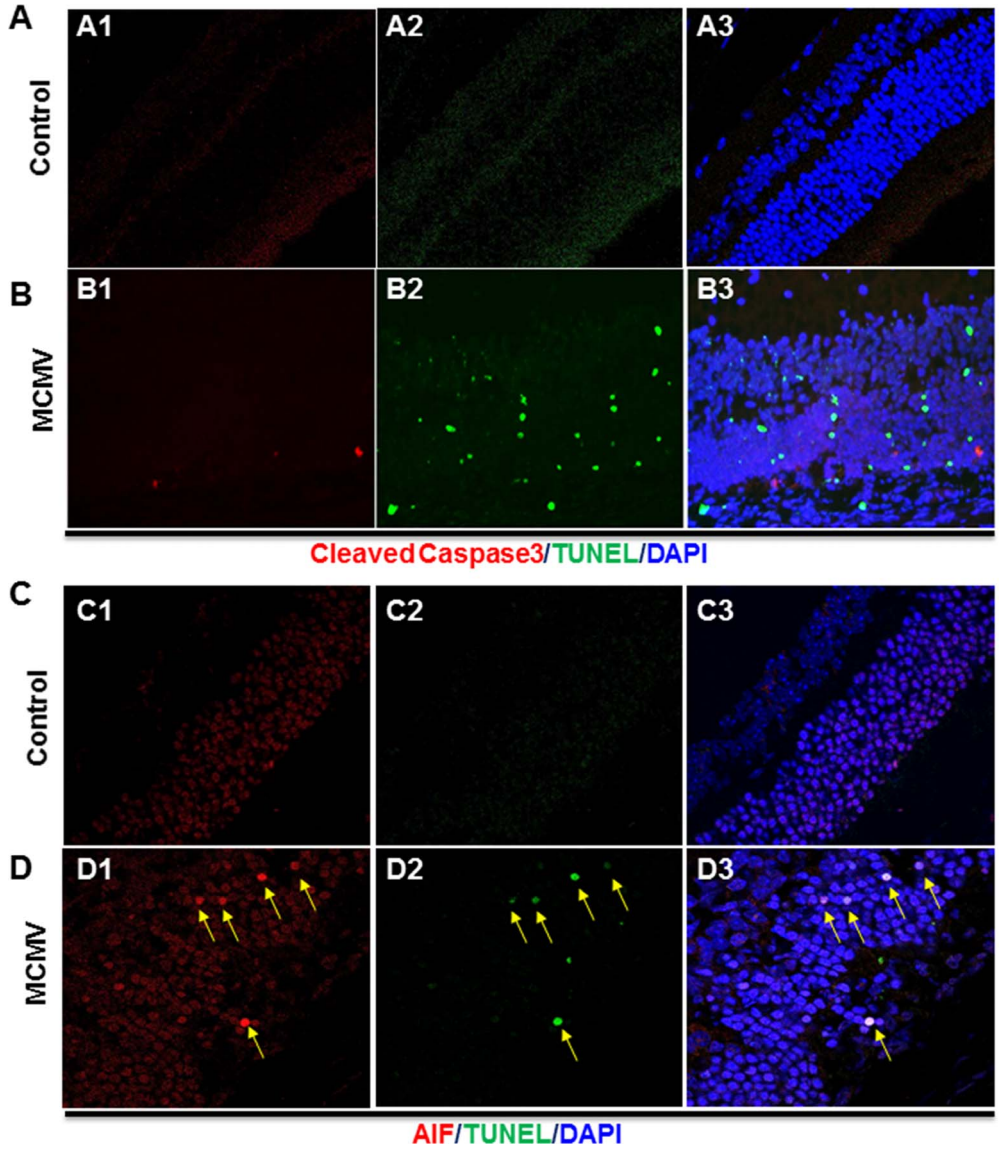

Figure 3. (**A**) Photomicrographs of cleaved caspase 3 (**A1**), TUNEL (**A2**), and DAPI staining in the mock-injected eye of an IS *Rip3*$^{+/+}$ mouse at day 7 p.i. As shown in the merged image (**A3**), no cleaved caspase 3– or TUNEL-stained cells were observed. (**B**) Photomicrographs of cleaved caspase 3 (**B1**), TUNEL (**B2**), and DAPI staining in the MCMV-injected eye of an IS *Rip3*$^{+/+}$ mouse. As shown in the merged image (**B3**), only a small number of cleaved caspase 3–stained cells were observed in the inner retina and the majority of TUNEL-stained cells did not have staining for cleaved caspase 3. (**C**) Photomicrographs of AIF (**C1**), TUNEL (**C2**), and DAPI staining in the mock-injected eye of an IS *Rip3*$^{+/+}$ mouse. As shown in the merged image (**C3**), no colocalization of AIF and DAPI was observed. (**D**) Photomicrographs of cleaved caspase 3 (**D1**), TUNEL (**D2**), and DAPI staining in the MCMV-injected eye of an IS *Rip3*$^{+/+}$ mouse. As shown in the merged image (**D3**), AIF was colocalized with DAPI in the majority of TUNEL-stained apoptotic cells in the outer nuclear layer (indicated by *arrows*).

colocalized with DAPI in the majority of TUNEL-positive apoptotic cells in the outer nuclear layer (Fig. 3D).

To determine if PARP1 activation was affected by RIP3 depletion, Western blots were performed to measure expression of PARP1. As shown in Figures 4A and 4B, less cleaved PARP1 was observed in MCMV-injected *Rip3*$^{-/-}$ eyes compared to MCMV-injected *Rip3*$^{+/+}$ eyes. In particular, at day 4 p.i., cleaved PARP1 was almost undetectable in MCMV-injected *Rip3*$^{-/-}$ eyes. To determine if calpain activation was also affected by *Rip3*$^{-/-}$ depletion, Western blots were performed to measure expression of calpain S1, a small 28-kDa regulatory subunit common to both calpain 1 and calpain 2,[37] and calpain degradation products (150 kDa) of α-fodrin. The results showed that less calpain S1 and cleaved α-fodrin were observed in MCMV-injected *Rip3*$^{-/-}$ eyes compared to MCMV-injected *Rip3*$^{+/+}$ eyes (Figs. 4C–E).

Caspase 3–Dependent Apoptosis

To determine if caspase 3–dependent apoptosis was also affected by RIP3 depletion, expression of cleaved caspase 3 was measured in infected eyes of *Rip3*$^{-/-}$ and *Rip3*$^{+/+}$ mice by Western blot. Cleaved caspase 3 was not present in mock-injected eyes of IS *Rip3*$^{-/-}$ and *Rip3*$^{+/+}$ mice, whereas in MCMV-injected eyes of both *Rip3*$^{-/-}$ and *Rip3*$^{+/+}$ mice, we observed the presence of cleaved caspase 3 (Fig. 5A). Quantification of band intensity indicated significantly lower amounts of cleaved caspase 3 in injected eyes of *Rip3*$^{-/-}$ mice than in injected eyes of *Rip3*$^{+/+}$ mice (Fig. 5B).

Investigative Ophthalmology & Visual Science

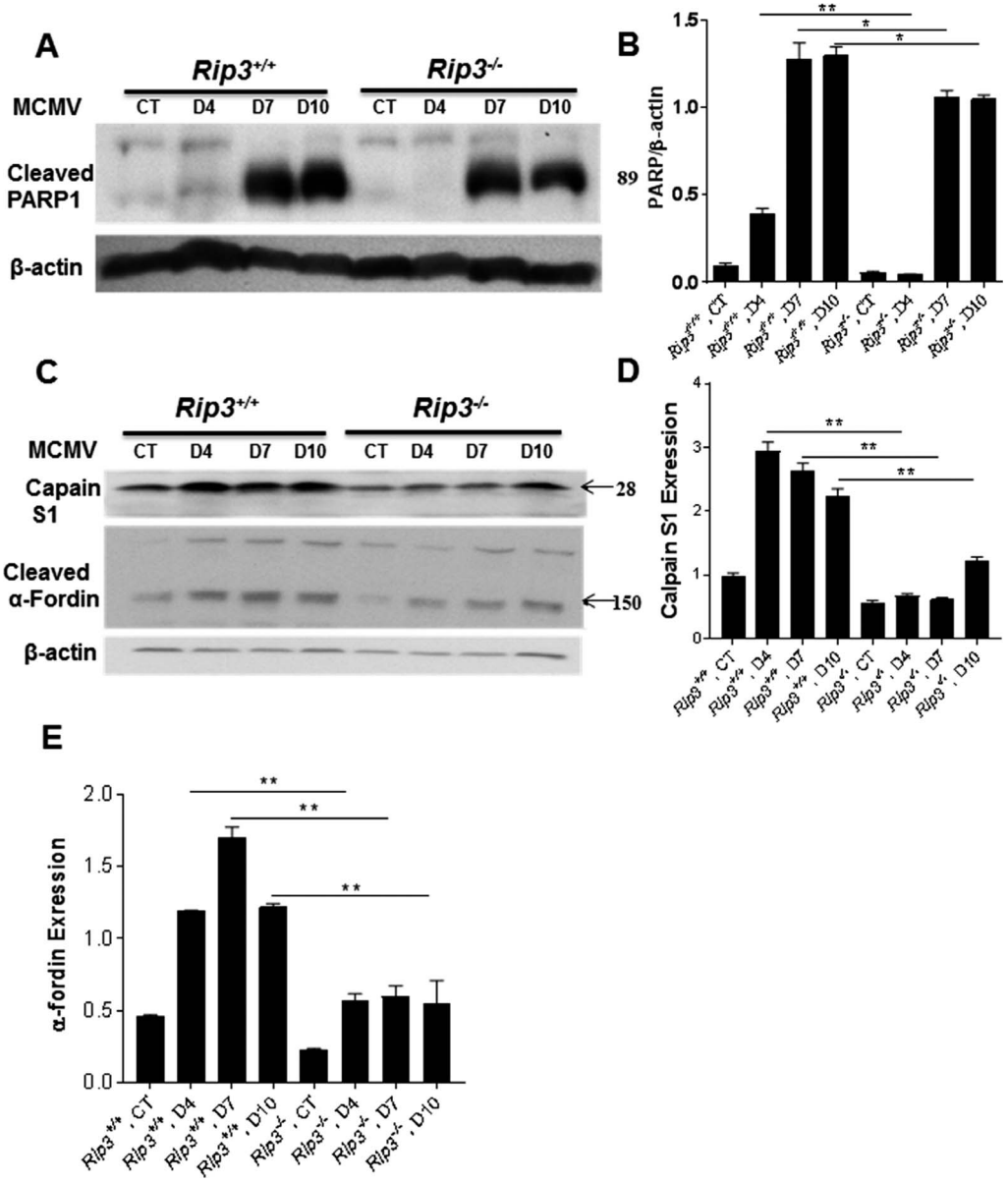

Figure 4. Western blot stained with antibodies against cleaved PARP1 (**A**), calpain S1 (**C**), and cleaved α-fodrin (**C**) in the injected eyes of mock-injected (CT) and MCMV-injected IS *Rip3*$^{+/+}$ or *Rip3*$^{-/-}$ mice at days 4, 7, and 10 p.i. Ratio of cleaved PARP1 to β-actin (**B**), calpain S1 to β-actin (**D**), and cleaved α-fodrin to β-actin (**E**). Data are shown as mean ± SEM ($n = 4$) and compared by ANOVA. $^{**}P < 0.01$, $^{*}P < 0.05$.

RIP3-Mediated Activation of Inflammasomes and NF-κB

RIP3 is an important factor for innate immune responses against bacteria and viruses through activation of the inflammasome or NF-κB.[24,38–42] The results presented here together with the results of other investigators[15,43] have demonstrated that depletion of RIP3 did not affect viral replication in systemic organs/tissues, whereas significantly more MCMV was recovered from the injected eyes of *Rip3*$^{-/-}$ mice than from the injected eyes of *Rip3*$^{+/+}$ mice. Based on these observations, we hypothesized that RIP3 might play an important role in the innate immune response against ocular MCMV infection by activation of caspase 1 or NF-κB.

Therefore, to test this hypothesis, relative levels of caspase 1 and NF-κB were measured in the injected eyes of *Rip3*$^{-/-}$ and *Rip3*$^{+/+}$ mice by Western blot. Expression of cleaved caspase 1 was increased after MCMV infection in *Rip3*$^{+/+}$ eyes as early as day 4 p.i. In contrast, increased levels of cleaved caspase 1 were found in *Rip3*$^{-/-}$ eyes only at day 10 p.i. (Fig. 5C). Quantification of band intensity indicated significantly lower amounts of cleaved caspase 1 in infected eyes of *Rip3*$^{-/-}$ mice compared to infected eyes of *Rip3*$^{+/+}$ mice at all time points tested p.i. (Fig. 5D). Our results also showed that depletion of RIP3 reduces NF-κB activation since NF-κB was activated earlier in *Rip3*$^{+/+}$ eyes compared to *Rip3*$^{-/-}$ eyes following MCMV infection (Fig. 5E). Significantly higher levels of active NF-κB were also observed in *Rip3*$^{+/+}$ eyes compared to *Rip3*$^{-/-}$ eyes at days 4, 7, and 10 p.i. (Fig. 5F).

Identification of Ocular Cells Exhibiting Increased RIP3 Expression Following MCMV Infection

To identify the cell types in which RIP3 was expressed, sections of MCMV-infected and uninfected control *Rip3*$^{+/+}$

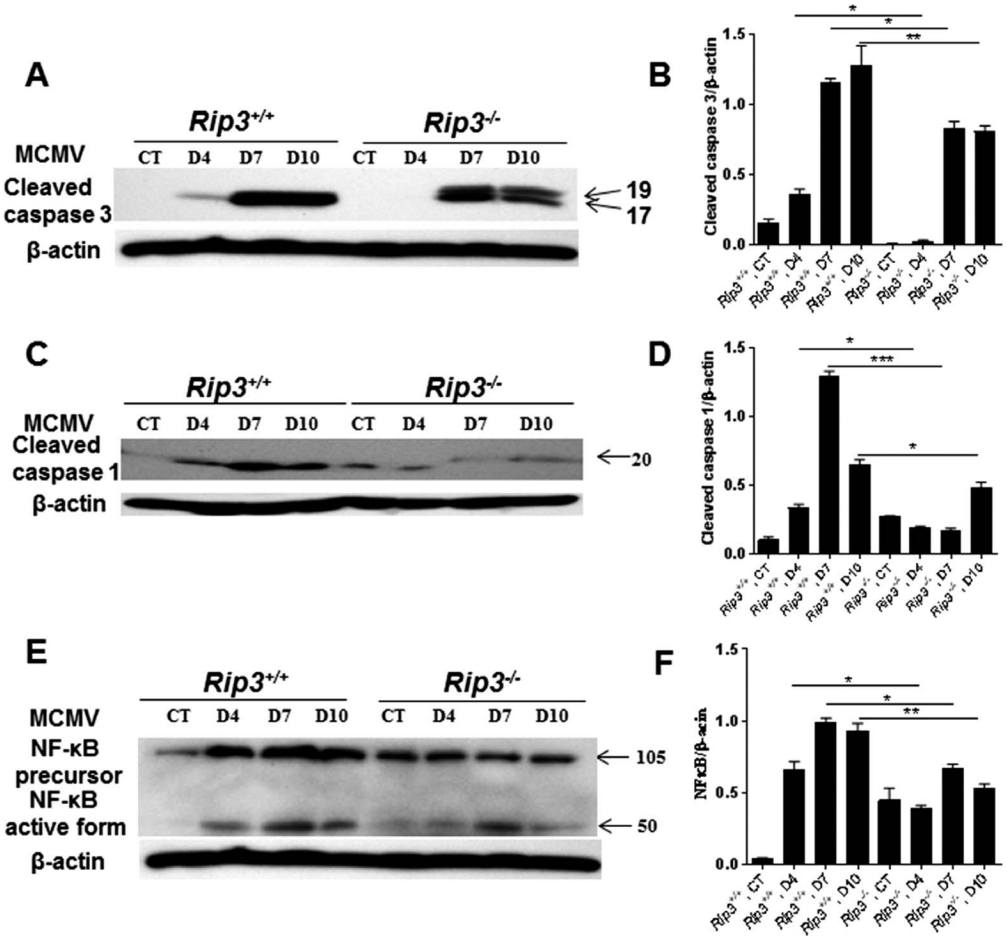

FIGURE 5. Western blot stained with antibodies against cleaved caspase 3 (**A**), cleaved caspase 1 (**C**), and NF-κB (**E**) in the injected eyes of mock-injected and MCMV-injected IS *Rip3*$^{+/+}$ or *Rip3*$^{-/-}$ mice at days 4, 7, and 10 p.i. Ratio of cleaved caspase 3 to β-actin (**B**), cleaved caspase 1 to β-actin (**D**), and NF-κB to β-actin (**F**). Data are shown as mean ± SEM ($n = 4$) and compared by ANOVA. $^{**}P < 0.01$, $^{*}P < 0.05$.

eyes were prepared at day 7 p.i. and double stained for RIP3 together with either MCMV EA, markers specific to various ocular and immune cells, or TUNEL assay. The results showed that retina neuronal antigens including rhodopsin (specific for photoreceptors) (Fig. 6A) and glycine (specific for amacrine cells) (Fig. 6B) were rarely colocalized with RIP3. Triple staining for RIP3, TUNEL, and rhodopsin (Fig. 6C) also showed that apoptotic photoreceptors were rarely colocalized with RIP3. RIP3 was almost undetectable in noninfected control eyes (Fig. 7A), whereas in contrast, many RIP3-expressing cells were observed in the choroid and pigmented RPE as well as in the inner retina of MCMV-injected eyes (Fig. 7B). IBA1 was expressed at high levels in infiltrating macrophages and microglia, and many IBA1-positive cells were present in the inner retina of MCMV-infected eyes. The majority of IBA1+ cells in MCMV-infected areas were also RIP3 positive while 40% of RIP3-positive cells in the inner retina of injected eyes were also IBA1 positive (Fig. 7C). Similarly, the majority of CD11b^{+} cells also stained positive for RIP3 (Fig. 7D). Since mice were IS, only a relatively small number of Gr-1+ neutrophils (Fig. 8A) and CD3^{+} T cells (Fig. 8B) were observed in the inner retina of MCMV-infected eyes, and therefore the majority of CD11b^{+} cells should be microglia/macrophages. In addition, no RIP3 staining was found among Gr-1–positive cells (Fig. 8A). Double staining for CD3 and RIP3 showed that some CD3^{+} T cells were RIP3 positive (Fig. 8B). In addition, double staining for GFAP and RIP3 showed that more than 40% of RIP3-positive cells in the inner retina of injected eyes were GFAP-positive glia/Müller cells (Fig. 8C). Although some RIP3-producing cells were observed in the outer nuclear layer, these cells were either IBA1-positive microglia/macrophages (Figs. 7C, 7D, indicated by arrows) or GFAP+ glia (Fig. 8C, indicated by arrows), but not rhodopsin-stained photoreceptors (Fig. 6A). Although many RIP3-producing cells were pigmented RPE cells (Fig. 7B, indicated by circles) or GFAP+ glia (Fig. 8C), the majority of MCMV-infected RPE cells (Fig. 7B) or infected glia (not shown) were either RIP3 negative (Fig. 7B, indicated by arrowheads) or stained only weakly for RIP3 (Fig. 7B, indicated by arrows).

DISCUSSION

The experiments presented herein demonstrate that RIP3 plays an important role in the innate immune response against ocular MCMV infection via activation of the inflammasome and NF-κB. Although an increased innate immune response and inflammation limit viral spread and replication in the retina, RIP3 is also responsible for the death of bystander retinal neuronal cells via multiple cell death pathways, particularly AIF-mediated, caspase-independent apoptosis.

The innate immune system is equipped with germline-encoded pattern recognition receptors (PRRs), which recognize pathogen-associated molecular patterns (PAMPS) and thus act as a first line of defense against pathogenic infection. When engaged by relevant PAMPs, these PRRs initiate signaling

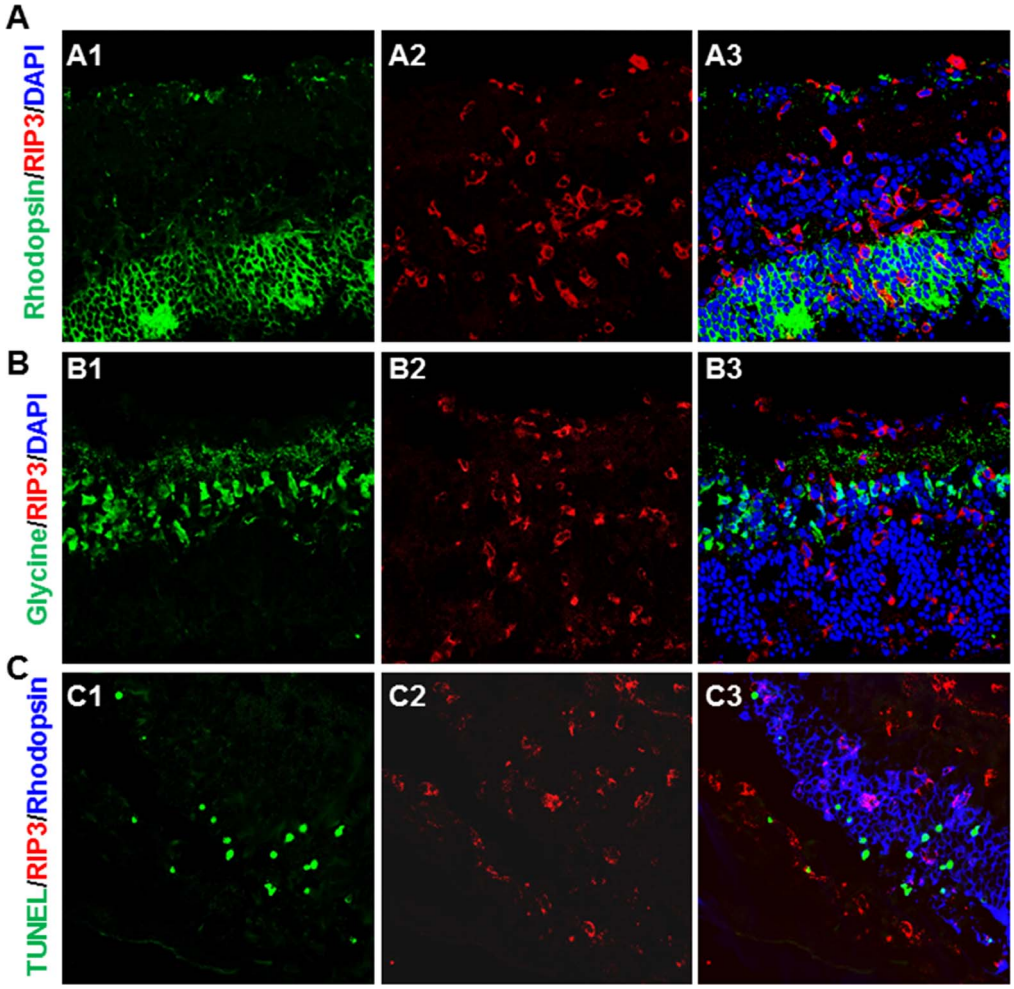

FIGURE 6. (**A**) Photomicrographs of rhodopsin (**A1**), RIP3 (**A2**), and DAPI staining in the MCMV-injected eye of an IS *Rip3*$^{+/+}$ mouse at day 7 p.i. As shown in the merged image (**A3**), rhodopsin+ photoreceptors were rarely colocalized with RIP3 staining. (**B**) Photomicrographs of glycine (**B1**), RIP3 (**B2**), and DAPI staining in the MCMV-injected eye of an IS *Rip3*$^{+/+}$ mouse at day 7 p.i. As shown in the merged image (**B3**), glycine-stained amacrine cells were rarely colocalized with RIP3 staining. (**C**) Photomicrographs of TUNEL (**C1**), RIP3 (**C2**), and rhodopsin staining in the MCMV-injected eye of an IS *Rip3*$^{+/+}$ mouse at day 7 p.i. As shown in the merged image (**C3**), TUNEL-stained cells in the outer nuclear layer were not colocalized with RIP3 staining.

pathways such as formation of the inflammasome and activation of the transcription factor NF-κB, resulting in the induction of immediate host defense mechanisms.[44] RIP1 mediates activation of NF-κB in response to a number of receptor systems including TNF-R1,[45,46] TRAIL,[47] Fas,[48] TLR3,[49,50] and TLR4.[50] In contrast, RIP3 is not responsible for (or does not even negatively regulate[42]) NF-κB signaling downstream of these receptor systems.[51] However, RIP1 and RIP3 synergize with each other to potentiate activation of NF-κB via interaction with DNA-sensor protein DAI, which represents one important mechanism of anti-viral immunity.[52,53] Inflammasomes are multiprotein complexes composed of caspase 1, the adaptor ASC1, and an upstream sensor such as NLRP3, that can activate caspase 1 and ultimately lead to the processing and secretion of downstream effectors, which drives the innate immune response.[54] RIP1 and RIP3 participate in activation of the inflammasome/caspase 1,[38,39,41,55] and several reports have also shown that RIP3 can facilitate inflammasome activation independently of necrosis.[38,39,41,56] However, RIP kinases have also been shown to play various tissue-specific roles,[57–60] and diverse models in the same organ have shown differing requirements for RIP1 and RIP3.[61]

The MCMV encoded protein M45 inhibits RIP3 phosphorylation, thus blocking subsequent RIP3 signaling through DAI and thereby preventing NF-κB activation.[62] Probably because of this RIP3 inhibition, the majority of MCMV-infected ocular cells including RPE cells and glia were RIP3 negative. However, RIP3 expression greatly increased in the nearby noninfected residential ocular cells including pigmented RPE cells, GFAP+ glia/Müller cells, and IBA1+ microglia/macrophages. RIP3 deficiency alone significantly reduced activation of caspase 1 and NF-kB and increased viral spread and replication in the retina. Interestingly, depletion of RIP3 does not affect viral spread and replication in extraocular organs/tissues including salivary glands, livers, or lungs, which is consistent with previous studies.[15,43] In our model, the majority of systemic immune cells including T cells, macrophages, and neutrophils were deleted,[63] and only a few neutrophils and T cells were observed in virus-infected eyes at early stages of infection. Taken together, we conclude from these results that (1) residential ocular cells including RPE cells, microglia, and glia/Müller cells play significant roles in the initial innate immune responses against virus infection in the retina and (2) RIP3 participates in activation of NF-κB and inflammasomes in these residential ocular cells.

Investigative Ophthalmology & Visual Science

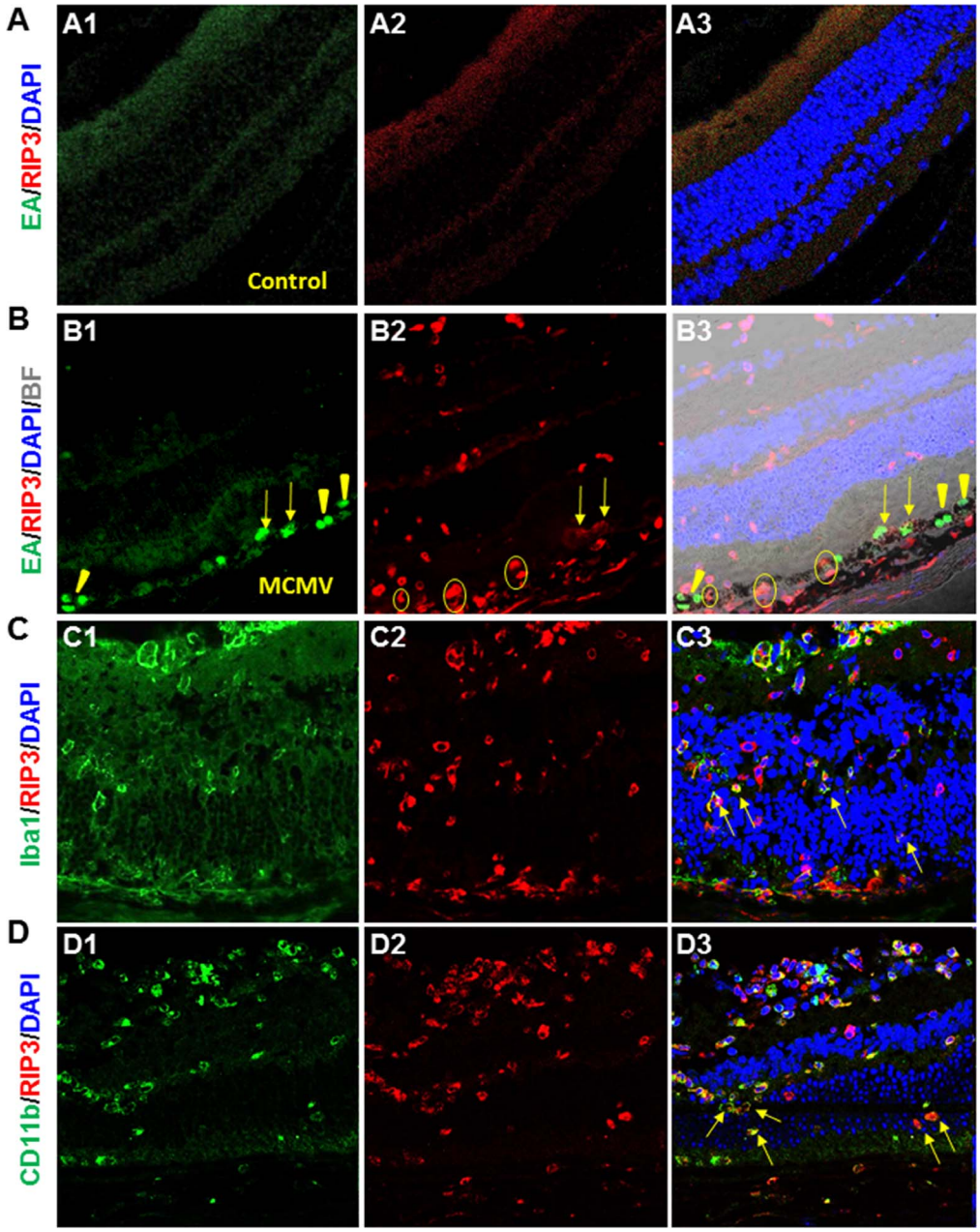

Figure 7. (**A**) Photomicrographs of MCMV EA (**A1**), RIP3 (**A2**), and DAPI staining in the mock-injected eye of an IS *Rip3*$^{+/+}$ mouse at day 7 p.i. As shown in the merged image (**A3**), MCMV EA and RIP3 staining was undetectable. (**B**) Photomicrographs of MCMV EA (**B1**), RIP3 (**B2**), and DAPI staining with brightfield in the MCMV-injected eye of an IS *Rip3*$^{+/+}$ mouse at day 7 p.i. As shown in the merged image (**B3**), many RIP3-expressing cells were observed in the choroid and pigmented RPE cells as well as in the inner retina of MCMV-injected eyes. Although many RIP3-producing cells were pigmented RPE cells (*circles*), the majority of MCMV-infected RPE cells did not stain with anti-RIP3 antibody (*arrowheads*) or stained only weakly (*arrows*). (**C**) Photomicrographs of IBA1 (**C1**), RIP3 (**C2**), and DAPI staining in the MCMV-injected eye of an IS *Rip3*$^{+/+}$ mouse at day 7 p.i. As shown in the merged image (**C3**), the majority of IBA1-stained microglia/macrophages in MCMV-infected areas also stained positive for RIP3. *Arrows* indicate RIP3-stained microglia/macrophages in the outer nuclear layer. (**D**) Photomicrographs of CD11b (**D1**), RIP3 (**D2**), and DAPI staining in the MCMV-injected eye of an IS *Rip3*$^{+/+}$ mouse at day 7 p.i. As shown in the merged image (**D3**), many CD11b-stained microglia/macrophages produced RIP3. *Arrows* indicate RIP3-stained microglia/macrophages in the outer nuclear layer.

RIP3 has emerged as a critical regulator of programmed necrosis/necroptosis,[29,64–68] which is often associated with inflammation, either pathogen induced or sterile. Activation of RIP3 is known to contribute to cell death in many diseases,[65] including several ocular diseases,[26,69–71] via MLKL-mediated necroptosis[65] or PARP1-AIF inducing necropsis/apoptosis.[70,72] It seems clear that death of uninfected retinal neurons contributes significantly to the pathogenesis of CMV retinitis,[12,13,17–24] and previous experiments performed in our laboratory have shown that both caspase 3–dependent and caspase 3–independent apoptosis contribute to retinal damage during MCMV retinitis.[12,18,23,25] Our results demonstrate that depletion of RIP3 not only decreases cell death via necrosis/necroptosis during MCMV retinitis, but also significantly reduces caspase 3–dependent and caspase 3–independent apoptosis, particularly AIF-mediated caspase 3–independent apoptotic cell death, a pathway traveled by the majority of bystander retinal neurons that subsequently died.[12,18,23,25]

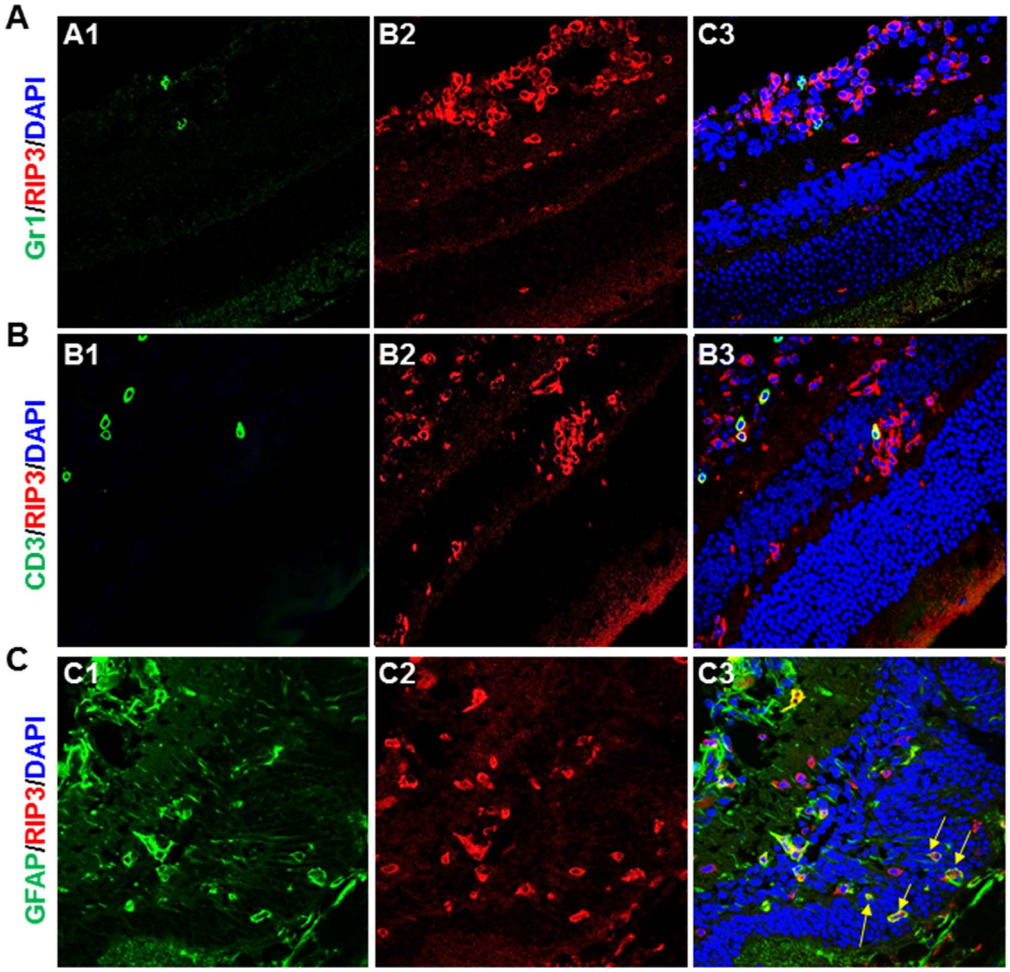

Figure 8. (**A**) Photomicrographs of Gr-1 (**A1**), RIP3 (**A2**), and DAPI staining in the MCMV-injected eye of an IS *Rip3*$^{+/+}$ mouse at day 7 p.i. As shown in the merged image (**A3**), a few Gr-1–stained neutrophils were observed in the inner retina but no RIP3 staining was detected in Gr-1–stained cells. (**B**) Photomicrographs of CD3 (**B1**), RIP3 (**B2**), and DAPI staining in the MCMV-injected eye of an IS *Rip3*$^{+/+}$ mouse at day 7 p.i. As shown in the merged image (**B3**), a few CD3-stained T cells were found in the inner retina and some also stained positive for RIP3. (**C**) Photomicrographs of GFAP (**C1**), RIP3 (**C2**), and DAPI staining in the MCMV-injected eye of an IS *Rip3*$^{+/+}$ mouse at day 7 p.i. As shown in the merged image (**C3**), many RIP3-stained cells in the inner retina of injected eyes also stained positive for GFAP, a marker for glia/Müller cells. *Arrows* indicate RIP3-stained glia/Müller cells in the outer nuclear layer.

AIF-mediated cell death has previously been shown to play a role in the death of neurons following exposure to cytotoxic agents in vivo.[33,73] AIF-mediated apoptotic-like cell death is associated with cleavage of AIF by calpains into a soluble form (tAIF) in response to endoplasmic reticulum (ER) stress, oxidative stress, or other specific lethal stimuli,[29–32] leading to its release from mitochondria and translocation into the nucleus, where it operates as an endonuclease to promote large-scale chromatin degradation.[74] AIF has also been implicated in PARP1-mediated necroptosis/apoptosis. PARP1 acts as a DNA nick sensor and upon activation, participates in DNA repair of single- or double-strand DNA breaks. Its hyperactivation by cellular insults can also trigger cell death. In PARP1-mediated necroptosis, PARP1 hyperactivation induces the depletion of NAD+, which has a dramatic bioenergetic impact including inhibition of mitochondrial ATP synthesis as well as glycolysis due to its impact on glyceraldehyde phosphate dehydrogenase.[29] Such a potent inhibition of ATP synthesis has been thought to constitute a sufficient cause for necrotic cell death.[29,75] PARP1-dependent necrosis relies on an additional molecular mechanism,[65,76] in which PARP1 hyperactivation results in the release of AIF from the mitochondrial intermembrane space (through the binding of AIF to PARP moieties[77]) followed by translocation to the nucleus, where its endonucleolytic activity results in profound degradation of chromatin.[74] However, necroptosis is not the only outcome of hyperactivated PARP1,[78–80] and depletion of NAD+ and energy reserves may not be enough for PARP1-mediated necrosis. Instead, depletion of NAD+ and energy reserves may be the trigger, which initiates apoptosis through AIF translocation.[34] Previous studies suggested that RIP3 can activate metabolic enzymes such as glutamate dehydrogenase 1, and thereby increase mitochondrial ROS production and act upstream of PARP1/AIF-mediated necroptosis/apoptosis.[70,72]

Interestingly, RIP3 was rarely detected in retinal neurons, including TUNEL-stained photoreceptors, during MCMV retinitis. In contrast, it was strongly expressed in ocular immune cells and was associated with activation of inflammasomes and NF-κB. This suggests that death of bystander retinal neurons may be triggered by activation of calpain or PARP1 due to oxidative or ER stress following an inflammatory response produced by ocular immune cells, rather than cell autonomous effects of RIP3.

Acknowledgments

Supported by National Institutes of Health Grant EY026642.

Disclosure: **J. Xu**, None; **J. Mo**, None; **X. Liu**, None; **B. Marshall**, None; **S.S. Atherton**, None; **Z. Dong**, None; **S. Smith**, None; **M. Zhang**, None

References

1. Cohen J. AIDS therapy. New hope against blindness. *Science*. 1995;268:368–369.
2. Drew WL. Cytomegalovirus infection in patients with AIDS. *Clin Infect Dis*. 1992;14:608–615.
3. Istas AS, Demmler GJ, Dobbins JG, Stewart JA. Surveillance for congenital cytomegalovirus disease: a report from the National Congenital Cytomegalovirus Disease Registry. *Clin Infect Dis*. 1995;20:665–670.
4. Jabs DA. Ocular manifestations of HIV infection. *Trans Am Ophthalmol Soc*. 1995;93:623–683.
5. Gallant JE, Moore RD, Richman DD, Keruly J, Chaisson RE; The Zidovudine Epidemiology Study Group. Incidence and natural history of cytomegalovirus disease in patients with advanced human immunodeficiency virus disease treated with zidovudine. *J Infect Dis*. 1992;166:1223–1227.
6. Shapira Y, Mimouni M, Vishnevskia-Dai V. Cytomegalovirus retinitis in HIV-negative patients - associated conditions, clinical presentation, diagnostic methods and treatment strategy [published online ahead of print October 25, 2017]. *Acta Ophthalmol*. doi:10.1111/aos.13553.
7. Sanghera NK, Newman TL. Cytomegaloviral retinitis from chronic immunosuppression following solid organ transplant surgery. *Clin Exp Optom*. 2010;93:261–263.
8. Jeon S, Lee WK, Lee Y, Lee DG, Lee JW. Risk factors for cytomegalovirus retinitis in patients with cytomegalovirus viremia after hematopoietic stem cell transplantation. *Ophthalmology*. 2012;119:1892–1898.
9. Palella FJ Jr, Delaney KM, Moorman AC, et al.; HIV Outpatient Study Investigators. Declining morbidity and mortality among patients with advanced human immunodeficiency virus infection. *New Engl J Med*. 1998;338:853–860.
10. Holtzer CD, Jacobson MA, Hadley WK, et al. Decline in the rate of specific opportunistic infections at San Francisco General Hospital, 1994-1997. *AIDS*. 1998;12:1931–1933.
11. Atherton SS, Newell CK, Kanter MY, Cousins SW. T cell depletion increases susceptibility to murine cytomegalovirus retinitis. *Invest Ophthalmol Vis Sci*. 1992;33:3353–3360.
12. Zhang M, Marshall B, Atherton SS. Murine cytomegalovirus infection and apoptosis in organotypic retinal cultures. *Invest Ophthalmol Vis Sci*. 2008;49:295–303.
13. Zhang M, Xin H, Roon P, Atherton SS. Infection of retinal neurons during murine cytomegalovirus retinitis. *Invest Ophthalmol Vis Sci*. 2005;46:2047–2055.
14. Handke W, Krause E, Brune W. Live or let die: manipulation of cellular suicide programs by murine cytomegalovirus. *Med Microbiol Immunol*. 2012;201:475–486.
15. Upton JW, Kaiser WJ, Mocarski ES. Virus inhibition of RIP3-dependent necrosis. *Cell Host Microbe*. 2010;7:302–313.
16. Ebermann L, Ruzsics Z, Guzman CA, et al. Block of death-receptor apoptosis protects mouse cytomegalovirus from macrophages and is a determinant of virulence in immunodeficient hosts. *PLoS Pathogens*. 2012;8:e1003062.
17. Bigger JE, Tanigawa M, Zhang M, Atherton SS. Murine cytomegalovirus infection causes apoptosis of uninfected retinal cells. *Invest Ophthalmol Vis Sci*. 2000;41:2248–2254.
18. Zhang M, Atherton SS. Apoptosis in the retina during MCMV retinitis in immunosuppressed BALB/c mice. *J Clin Virol*. 2002;25(suppl 2):S137–S147.
19. Zhou J, Zhang M, Atherton SS. Tumor necrosis factor-alpha-induced apoptosis in murine cytomegalovirus retinitis. *Invest Ophthalmol Vis Sci*. 2007;48:1691–1700.
20. Chiou SH, Liu JH, Hsu WM, et al. Up-regulation of Fas ligand expression by human cytomegalovirus immediate-early gene product 2: a novel mechanism in cytomegalovirus-induced apoptosis in human retina. *J Immunol*. 2001;167:4098–4103.
21. Buggage RR, Chan CC, Matteson DM, Reed GF, Whitcup SM. Apoptosis in cytomegalovirus retinitis associated with AIDS. *Curr Eye Res*. 2000;21:721–729.
22. Chiou SH, Liu JH, Chen SS, et al. Apoptosis of human retina and retinal pigment cells induced by human cytomegalovirus infection. *Ophthalmic Res*. 2002;34:77–82.
23. Zhang M, Covar J, Marshall B, Dong Z, Atherton SS. Lack of TNF-alpha promotes caspase-3-independent apoptosis during murine cytomegalovirus retinitis. *Invest Ophthalmol Vis Sci*. 2011;52:1800–1808.
24. Dix RD, Cousins SW. Susceptibility to murine cytomegalovirus retinitis during progression of MAIDS: correlation with intraocular levels of tumor necrosis factor-alpha and interferon-gamma. *Curr Eye Res*. 2004;29:173–180.
25. Mo J, Marshall B, Covar JA, et al. Role of Bax in death of uninfected retinal cells during murine cytomegalovirus (MCMV) retinitis. *Invest Ophthalmol Vis Sci*. 2014;55:7137–7146.
26. Chien H, Dix RD. Evidence for multiple cell death pathways during development of experimental cytomegalovirus retinitis in mice with retrovirus-induced immunosuppression: apoptosis, necroptosis, and pyroptosis. *J Virol*. 2012;86:10961–10978.
27. Pande H, Campo K, Shanley JD, et al. Characterization of a 52K protein of murine cytomegalovirus and its immunological cross-reactivity with the DNA-binding protein ICP36 of human cytomegalovirus. *J Gen Virol*. 1991;72(pt 6):1421–1427.
28. Zhang M, Zhou J, Marshall B, Xin H, Atherton SS. Lack of iNOS facilitates MCMV spread in the retina. *Invest Ophthalmol Vis Sci*. 2007;48:285–292.
29. Galluzzi L, Kepp O, Krautwald S, Kroemer G, Linkermann A. Molecular mechanisms of regulated necrosis. *Semin Cell Dev Biol*. 2014;35:24–32.
30. Cande C, Vahsen N, Kouranti I, et al. AIF and cyclophilin A cooperate in apoptosis-associated chromatinolysis. *Oncogene*. 2004;23:1514–1521.
31. Zhu C, Wang X, Huang Z, et al. Apoptosis-inducing factor is a major contributor to neuronal loss induced by neonatal cerebral hypoxia-ischemia. *Cell Death Differ*. 2007;14:775–784.
32. Susin SA, Lorenzo HK, Zamzami N, et al. Molecular characterization of mitochondrial apoptosis-inducing factor. *Nature*. 1999;397:441–446.
33. Delavallee L, Cabon L, Galan-Malo P, Lorenzo HK, Susin SA. AIF-mediated caspase-independent necroptosis: a new chance for targeted therapeutics. *IUBMB Life*. 2011;63:221–232.
34. Yu SW, Wang H, Poitras MF, et al. Mediation of poly(ADP-ribose) polymerase-1-dependent cell death by apoptosis-inducing factor. *Science*. 2002;297:259–263.
35. Baritaud M, Boujrad H, Lorenzo HK, Krantic S, Susin SA. Histone H2AX: the missing link in AIF-mediated caspase-independent programmed necrosis. *Cell Cycle*. 2010;9:3166–3173.
36. Boujrad H, Gubkina O, Robert N, Krantic S, Susin SA. AIF-mediated programmed necrosis: a highly regulated way to die. *Cell Cycle*. 2007;6:2612–2619.
37. Goll DE, Thompson VF, Li H, Wei W, Cong J. The calpain system. *Physiol Rev*. 2003;83:731–801.
38. Weng D, Marty-Roix R, Ganesan S, et al. Caspase-8 and RIP kinases regulate bacteria-induced innate immune responses and cell death. *Proc Natl Acad Sci U S A*. 2014;111:7391–7396.

Investigative Ophthalmology & Visual Science

39. Vince JE, Wong WW, Gentle I, et al. Inhibitor of apoptosis proteins limit RIP3 kinase-dependent interleukin-1 activation. *Immunity.* 2012;36:215–227.
40. Blalock EL, Chien H, Dix RD. Murine cytomegalovirus downregulates interleukin-17 in mice with retrovirus-induced immunosuppression that are susceptible to experimental cytomegalovirus retinitis. *Cytokine*. 2013;61:862–875.
41. Philip NH, Dillon CP, Snyder AG, et al. Caspase-8 mediates caspase-1 processing and innate immune defense in response to bacterial blockade of NF-kappaB and MAPK signaling. *Proc Natl Acad Sci U S A*. 2014;111:7385–7390.
42. Sun X, Lee J, Navas T, Baldwin DT, Stewart TA, Dixit VM. RIP3, a novel apoptosis-inducing kinase. *J Biol Chem*. 1999;274:16871–16875.
43. Upton JW, Kaiser WJ, Mocarski ES. DAI/ZBP1/DLM-1 complexes with RIP3 to mediate virus-induced programmed necrosis that is targeted by murine cytomegalovirus vIRA. *Cell Host Microbe*. 2012;11:290–297.
44. Vajjhala PR, Ve T, Bentham A, Stacey KJ, Kobe B. The molecular mechanisms of signaling by cooperative assembly formation in innate immunity pathways. *Mol Immunol*. 2017;86:23–37.
45. Ting AT, Pimentel-Muinos FX, Seed B. RIP mediates tumor necrosis factor receptor 1 activation of NF-kappaB but not Fas/APO-1-initiated apoptosis. *EMBO J*. 1996;15:6189–6196.
46. Kelliher MA, Grimm S, Ishida Y, Kuo F, Stanger BZ, Leder P. The death domain kinase RIP mediates the TNF-induced NF-kappaB signal. *Immunity.* 1998;8:297–303.
47. Lin Y, Devin A, Cook A, et al. The death domain kinase RIP is essential for TRAIL (Apo2L)-induced activation of IkappaB kinase and c-Jun N-terminal kinase. *Mol Cell Biol*. 2000;20:6638–6645.
48. Kreuz S, Siegmund D, Rumpf JJ, et al. NFkappaB activation by Fas is mediated through FADD, caspase-8, and RIP and is inhibited by FLIP. *J Cell Biol*. 2004;166:369–380.
49. Meylan E, Burns K, Hofmann K, et al. RIP1 is an essential mediator of Toll-like receptor 3-induced NF-kappa B activation. *Nat Immunol*. 2004;5:503–507.
50. Cusson-Hermance N, Khurana S, Lee TH, Fitzgerald KA, Kelliher MA. Rip1 mediates the Trif-dependent toll-like receptor 3- and 4-induced NF-{kappa}B activation but does not contribute to interferon regulatory factor 3 activation. *J Biol Chem*. 2005;280:36560–36566.
51. Newton K, Sun X, Dixit VM. Kinase RIP3 is dispensable for normal NF-kappa Bs, signaling by the B-cell and T-cell receptors, tumor necrosis factor receptor 1, and Toll-like receptors 2 and 4. *Mol Cell Biol*. 2004;24:1464–1469.
52. Kaiser WJ, Upton JW, Mocarski ES. Receptor-interacting protein homotypic interaction motif-dependent control of NF-kappa B activation via the DNA-dependent activator of IFN regulatory factors. *J Immunol*. 2008;181:6427–6434.
53. Mocarski ES, Kaiser WJ, Livingston-Rosanoff D, Upton JW, Daley-Bauer LP. True grit: programmed necrosis in antiviral host defense, inflammation, and immunogenicity. *J Immunol*. 2014;192:2019–2026.
54. Jacobs SR, Damania B. NLRs, inflammasomes, and viral infection. *J Leukoc Biol*. 2012;92:469–477.
55. Kataoka K, Matsumoto H, Kaneko H, et al. Macrophage- and RIP3-dependent inflammasome activation exacerbates retinal detachment-induced photoreceptor cell death. *Cell Death Dis*. 2015;6:e1731.
56. Dix RD, Cousins SW. Interleukin-2 immunotherapy of murine cytomegalovirus retinitis during MAIDS correlates with increased intraocular CD8+ T-cell infiltration. *Ophthalmic Res*. 2003;35:154–159.
57. Rickard JA, O'Donnell JA, Evans JM, et al. RIPK1 regulates RIPK3-MLKL-driven systemic inflammation and emergency hematopoiesis. *Cell*. 2014;157:1175–1188.
58. Silke J, Rickard JA, Gerlic M. The diverse role of RIP kinases in necroptosis and inflammation. *Nat Immunol*. 2015;16:689–697.
59. Kumari S, Redouane Y, Lopez-Mosqueda J, et al. Sharpin prevents skin inflammation by inhibiting TNFR1-induced keratinocyte apoptosis. *Elife*. 2014;3:e03422.
60. Rickard JA, Anderton H, Etemadi N, et al. TNFR1-dependent cell death drives inflammation in Sharpin-deficient mice. *Elife*. 2014;3:e03464.
61. Deutsch M, Graffeo CS, Rokosh R, et al. Divergent effects of RIP1 or RIP3 blockade in murine models of acute liver injury. *Cell Death Dis*. 2015;6:e1759.
62. Rebsamen M, Heinz LX, Meylan E, et al. DAI/ZBP1 recruits RIP1 and RIP3 through RIP homotypic interaction motifs to activate NF-kappaB. *EMBO Rep*. 2009;10:916–922.
63. Duan Y, Ji Z, Atherton SS. Dissemination and replication of MCMV after supraciliary inoculation in immunosuppressed BALB/c mice. *Invest Ophthalmol Vis Sci*. 1994;35:1124–1131.
64. Christofferson DE, Li Y, Hitomi J, et al. A novel role for RIP1 kinase in mediating TNFalpha production. *Cell Death Dis*. 2012;3:e320.
65. Christofferson DE, Yuan J. Necroptosis as an alternative form of programmed cell death. *Curr Opin Cell Biol*. 2010;22:263–268.
66. Cregan SP, Fortin A, MacLaurin JG, et al. Apoptosis-inducing factor is involved in the regulation of caspase-independent neuronal cell death. *J Cell Biol*. 2002;158:507–517.
67. Moubarak RS, Yuste VJ, Artus C, et al. Sequential activation of poly(ADP-ribose) polymerase 1, calpains, and Bax is essential in apoptosis-inducing factor-mediated programmed necrosis. *Mol Cell Biol*. 2007;27:4844–4862.
68. Xu Y, Huang S, Liu ZG, Han J. Poly(ADP-ribose) polymerase-1 signaling to mitochondria in necrotic cell death requires RIP1/TRAF2-mediated JNK1 activation. *J Biol Chem*. 2006;281:8788–8795.
69. Sato K, Li S, Gordon WC, et al. Receptor interacting protein kinase-mediated necrosis contributes to cone and rod photoreceptor degeneration in the retina lacking interphotoreceptor retinoid-binding protein. *J Neurosci*. 2013;33:17458–17468.
70. Trichonas G, Murakami Y, Thanos A, et al. Receptor interacting protein kinases mediate retinal detachment-induced photoreceptor necrosis and compensate for inhibition of apoptosis. *Proc Natl Acad Sci U S A*. 2010;107:21695–21700.
71. Viringipurampeer IA, Shan X, Gregory-Evans K, Zhang JP, Mohammadi Z, Gregory-Evans CY. Rip3 knockdown rescues photoreceptor cell death in blind pde6c zebrafish. *Cell Death Differ*. 2014;21:665–675.
72. Zhang DW, Shao J, Lin J, et al. RIP3, an energy metabolism regulator that switches TNF-induced cell death from apoptosis to necrosis. *Science*. 2009;325:332–336.
73. Polster BM. AIF, reactive oxygen species, and neurodegeneration: a "complex" problem. *Neurochem Int*. 2013;62:695–702.
74. Linkermann A, Heller JO, Prokai A, et al. The RIP1-kinase inhibitor necrostatin-1 prevents osmotic nephrosis and contrast-induced AKI in mice. *J Am Soc Nephrol*. 2013;24:1545–1557.
75. Chiarugi A. Intrinsic mechanisms of poly(ADP-ribose) neurotoxicity: three hypotheses. *Neurotoxicology.* 2005;26:847–855.
76. Ofengeim D, Yuan J. Regulation of RIP1 kinase signalling at the crossroads of inflammation and cell death. *Nat Rev Mol Cell Biol*. 2013;14:727–736.
77. Wang Y, Kim NS, Haince JF, et al. Poly(ADP-ribose) (PAR) binding to apoptosis-inducing factor is critical for PAR

polymerase-1-dependent cell death (parthanatos). *Sci Signal*. 2011;4:ra20.

78. Wang X, Wang Y, Ding ZJ, et al. The role of RIP3 mediated necroptosis in ouabain-induced spiral ganglion neurons injuries. *Neurosci Lett*. 2014;578C:111–116.
79. Wang Y, Wang H, Tao Y, Zhang S, Wang J, Feng X. Necroptosis inhibitor necrostatin-1 promotes cell protection and physiological function in traumatic spinal cord injury. *Neuroscience*. 2014;266:91–101.
80. Zhang L, Jiang F, Chen Y, et al. Necrostatin-1 attenuates ischemia injury induced cell death in rat tubular cell line NRK-52E through decreased Drp1 expression. *Int J Mol Sci*. 2013; 14:24742–24754.

Investigative Ophthalmology & Visual Science